The disruption of invariant natural killer T cells exacerbates cardiac hypertrophy and failure due to pressure overload in mice

by Mochamad Ali Sobirin

Submission date: 23-Jan-2020 10:05AM (UTC+0700)
Submission ID: 1245211334
File name: Experimental_physiology_mochamad_ali_sobirin_2020.pdf (1.6M)
Word count: 7544
Character count: 40801

Natural killer T cells and heart failure

DOI: 10.1113/EP087652

The disruption of invariant natural killer T cells exacerbates cardiac hypertrophy and failure due to pressure overload in mice

Masashige Takahashi,[1] Shintaro Kinugawa,[1,*] Shingo Takada,[1] Naoya Kakutani[1], Takaaki Furihata,[1] Mochamad Ali Sobirin,[2] Arata Fukushima,[1] Yoshikuni Obata,[1] Akimichi Saito,[1] Naoki Ishimori,[1] Kazuya Iwabuchi,[3] and Hiroyuki Tsutsui[4]

[1]Department of Cardiovascular Medicine, Faculty of Medicine and Graduate School of Medicine, Hokkaido University, Sapporo 0608638, Japan

[2]Faculty of Medicine, Diponegoro University, Semarang 1269, Indonesia

[3]Department of Immunobiology, Kitasato University School of Medicine, Kanagawa 2520374, Japan

[4]Department of Cardiovascular Medicine, Faculty of Medical Sciences, Kyushu University, Fukuoka 8128582, Japan

***Corresponding author:** Dr. Shintaro Kinugawa, Department of Cardiovascular Medicine, Faculty of Medicine and Graduate School of Medicine, Hokkaido University, Kita-15, Nishi-7, Kita-ku, Sapporo 060-8638, Japan. Email: tuckahoe@med.hokudai.ac.jp

Key words: hypertrophy, natural killer T cells, inflammation, cardiac hypertrophy, cardiac failure

This is an Accepted Article that has been peer-reviewed and approved for publication in the Experimental Physiology, but has yet to undergo copy-editing and proof correction. Please cite this article as an Accepted Article; doi: 10.1113/EP087652.

Total number of words: 6626 words, Total number of references: 48

ABSTRACT

Chronic inflammation is involved in the development of cardiac remodeling and heart failure (HF). Invariant natural killer T (iNKT) cells, a subset of T lymphocytes, have been shown to produce various cytokines and orchestrate tissue inflammation. The pathophysiological role of iNKT cells in HF due to pressure overload has not been studied. Here, we investigated whether the disruption of iNKT cells affected this process in mice. Transverse aortic constriction (TAC) and a sham operation were performed in male C57BL/6J wild-type (WT) and iNKT cell-deficient Jα18 knockout (KO) mice. The infiltration of iNKT cells was increased after TAC. The disruption of iNKT cells exacerbated left ventricular (LV) remodeling and hastened the transition to HF after TAC. Histological examinations also revealed that the disruption of iNKT cells induced worsened myocyte hypertrophy and a further increase in interstitial fibrosis after TAC. The expressions of interleukin-10 and tumor necrosis factor-α mRNA and their ratio in the LV after TAC were decreased in the KO compared to WT mice, which may indicate that the disruption of iNKT cells leads to an imbalance between T-helper type 1 and type 2 cytokines. The phosphorylation of ERK was significantly increased in the KO mice. The disruption of iNKT cells exacerbated the development of cardiac remodeling and HF after TAC. The activation of iNKT cells may play a protective role against HF due to pressure overload. Targeting the activation of iNKT cells may thus be a promising candidate as a new therapeutic strategy for HF.

New Findings

What is the central question of this study?

We addressed the question of whether the disruption of iNKT cells exacerbates LV remodeling and HF after TAC in mice.

What are the main findings and their importance?

Pressure overload by transverse aortic constriction increased the infiltration of iNKT cells in mouse heart. The disruption of iNKT cells exacerbated LV remodeling and hastened the

transition to heart failure from hypertrophy in association with the activation of MAPK signaling. The activation of iNKT cells modulated the immunological balance in this process and played a protective role against LV remodeling and failure.

1. INTRODUCTION

Left ventricular (LV) hypertrophy in response to pressure overload is an initially adaptive process that normalizes wall stress and preserves contractile performance. However, sustained mechanical stress can result in the progression to maladaptive hypertrophy and cause the development of cardiac remodeling and heart failure (HF). Various molecular mechanisms underlying maladaptive hypertrophy and HF in response to mechanical stress are known, and several pro-inflammatory cytokines including interleukin (IL)-6 and tumor necrosis factor-alpha (TNF-α) have important roles in these mechanisms (Fischer & Hilfiker-Kleiner, 2007; Sun et al., 2007).

It has been reported that pressure overload as well as ischemia induces cardiac inflammation in association with the upregulation of chemokines and the infiltration of inflammatory cells, and this have important roles in the development of cardiac fibrosis (Nicoletti & Michel, 1999; Xia et al., 2009). In contrast, chronic inflammation was also reported to have protective effects during the maladaptive transition from hypertrophy to HF (Hirota et al., 1999; Higuchi et al., 2004). These findings suggested that (1) cardiac inflammation may have bi-directional roles in the pathophysiology of HF, and (2) the immunological modulation of a comprehensive cytokine network rather than the regulation of a single cytokine may be a suitable treatment strategy for patients with HF.

Invariant natural killer T (iNKT) cells are an innate-like T lymphocyte population that recognizes glycolipid ligands in the context of the protein CD1d. These cells are characterized by the co-expression of NK markers and the lipid-specific T-cell receptor (TCR) combined with a canonical Vα14-Jα18 chain with the variable Vβ8, -7, or -2 in mice or Vβ8, -11 in humans (Kronenberg & Gapin, 2002; Godfrey et al., 2004). The synthetic glycolipid α-galactosylceramide (αGC) specifically activates CD1d-restricted iNKT cells (Kawano et 1997). Upon activation, the iNKT cells have the capacity to rapidly secrete a mixture of large amounts of T-helper type 1 (T_H1) and T_H2 cytokines plus a vast array of chemokines that

the subsequent adaptive immune response (Matsuda et al., 2008). Thus, iNKT cells can function as a bridge between the innate and adaptive immune systems, and very few iNKT adequately conduct various immune cells and orchestrate tissue inflammation.

Indeed, iNKT cells are known to play a protective role in autoimmune and inflammatory diseases such as type 1 diabetes, experimental allergic encephalomyelitis, and rheumatoid arthritis (Hong et al., 2001; Sharif et al., 2001; Singh et al., 2001; Miellot et al., 2005). We reported that the activation of iNKT cells by αGC ameliorated cardiac remodeling and HF after myocardial infarction (MI) in mice (Sobirin et al., 2012). However, to date, no studies have examined the pathophysiological roles of iNKT cells in the development of cardiac hypertrophy and HF.

In the present study, we evaluated the effects of a targeted deletion of iNKT gene on mortality and LV structural and functional alterations during pressure-overloaded cardiac hypertrophy. We used Jα18$^{-/-}$ (formerly called Jα28$^{-/-}$) mice with the targeted disruption of the Jα18 gene, resulting in the selective depletion of CD1d-dependent Vα14 iNKT cells (Cui et al., 1997; Rogers et al., 2008).

2. METHODS

2.1. Ethical approval

All procedures and animal care in this study (16-0101) were approved by Hokkaido University Graduate School of Medicine Committee on Animal Resources and conformed to the guiding principles in the care and use of animals of the American Physiological Society and the Guide for the Care and Use of Laboratory Animals of the National Research Council. At the end of the experiment, the mice were anaesthetized by overdose of pentobarbital sodium (100 mg/kg) and killed by collection of blood from abdominal aorta.

2.2. Animals and experimental protocol

Vα14^{+} NKT cell-deficient Jα18$^{-/-}$ (KO) mice were provided from Dr. M. Taniguchi (RIKEN, Yokohama, Japan) and backcrossed 10 times to C57BL/6J. C57BL/6J wild-type (WT) mice and KO mice bred in a pathogen-free environment. All experiments were performed using male mice. All mice were 12–15 weeks old when they were used for the experiments. The mice were kept under a constant 12-hr light/dark cycle at a temperature of 23°–25°C. Standard chow and water were provided.

The transverse aortic constriction (TAC) procedure was performed in WT (WT+TAC; n=15) or KO (KO+TAC; n=22) mice as described (Furihata et al., 2016). Briefly, after being anesthetized with an intraperitoneal injection of a mixture of 0.3 mg/kg of medetomidine (Dorbene®, Kyoritsuseiyaku, Tokyo), 4.0 mg/kg of midazolam (Dormicum®, Astellas Pharma, Tokyo), and 5.0 mg/kg of butorphanol (Vetorphale®, Meiji Seika Kaisha, Tokyo), the mouse was intubated and its respiration was assisted with a volume-cycled ventilator (Shinano Co., Tokyo) connected to a 21-gauge cannula inserted into the trachea under the condition of 120 breaths/min and 0.3 mL tidal volume. A thoracotomy was performed via the second internal costal space at the left upper sternal border. The transverse aortic arch was isolated and ligated between the innominate and left common carotid arteries with an overlying 28-gauge needle, which, after removal of the needle, left a reproducible discrete region of stenosis. After surgery, we subcutaneously administered 5mg/kg of meloxicam (Metacam®, Boehringer Ingelheim, Tokyo) as an analgesia to mice.

A sham operation without realizing aortic stenosis was performed in WT (WT+Sham; n=7) and KO (KO+Sham; n=7) mice. During the study period of 2 weeks after surgery, the cages were inspected daily for deceased animals. Mice that did not eat meals and became immobilized early after surgery were euthanized and excluded from the analysis. Euthanasia was performed in four WT+TAC mice and six KO+TAC mice.

Echocardiographic, hemodynamic, and organ weight measurements were performed in the survived mice (WT+Sham, n=7; KO+Sham, n=7; WT+TAC, n=10; and KO+TAC, Due to technical reasons, hemodynamic data could not be measured in some mice. After the mice were sacrificed, hearts from mice were used for the histological analysis, the immunohistochemical analysis, and the quantitative reverse transcriptase polymerase chain reaction (PCR) (n=4–9 for each group). Because heart samples from mice are limited in

volume, for the flow cytometry analysis (n=15, each group) and immunoblotting (n=3–5, group), additional mice different mice from the above mice were used. n represents the of mice, and data taken multiple time from the same mice are not included.

2.3. Isolation of cardiac mononuclear cells

LV tissue was harvested, minced with a fine scissors, placed in 10 ml of RPMI-1640 with 5% fetal bovine serum (FBS), 1 mg/ml collagenase type IV, and 100 U/ml DNase I, shaken at 37°C for 45 min, and then triturated through 70-μm nylon mesh and centrifuged (1,400 rpm for 5 min at 4°C). Red blood cells were lysed with Tris-ammonium chloride for 1 min at room temperature. Cardiac mononuclear cells (MNCs) were isolated by density-gradient centrifugation with 12 ml of 33% Percoll™ as described (Sobirin et al., 2012; Homma et al., 2013). Cardiac MNCs from five mice were pooled and subjected to a flow cytometric analysis. All reagents were purchased from Sigma-Aldrich (St. Louis, MO). Cardiac cell numbers were determined with Trypan blue (Wako Pure Chemical Industries, Osaka, Japan).

2.4. Flow cytometry

To detect iNKT cells, we performed a flow cytometry analysis as we described (Sobirin et al., 2012; Homma et al., 2013). Cells were incubated with 2.4G2 monoclonal antibody to block the non-specific binding of the primary monoclonal antibody, and then the cells were reacted with αGC-loaded Dimer X (CD1d: Ig recombinant fusion protein), followed by their detection with phycoerythrin-conjugated anti-mouse IgG1 monoclonal antibody. After being washed, the cells were stained with a combination of fluorescein isothiocyanate-anti-T-cell receptor (TCR) β and phycoerythrin-anti-mouse IgG1. These antibodies (except 2.4G2 monoclonal antibody) were purchased from BD Bioscience Pharmingen (San Diego, CA).

Stained cells were acquired with a FACS Canto II Flow Cytometer (BD Biosciences Immunocytometry Systems, San Jose, CA) and analyzed with FlowJo ver. 7.2.5 software (Flow Jo, Ashland, OR). Propidium iodide (Sigma-Aldrich)-positive cells were electronically

gated out from the analysis as dead cells. Each sample population was classified for cell size (forward scatter) and complexity (side scatter), then gated on a population of interest. At least 1.0×10^4 cells were evaluated for each sample. The proportion of Dimer X^+ TCRβ^+ cells was calculated as the percentage of Dimer X^+TCRβ^+ cells among TCRβ^+ cells.

2.5. Echocardiographic and hemodynamic measurements

Echocardiographic and hemodynamic measurements of the mice were performed under anesthesia with 2-3% isoflurane inhalation. A two-dimensional parasternal short-axis view was obtained at the levels of the papillary muscles. In general, the best views were obtained with the transducer lightly applied to the mid-upper left anterior chest wall. The transducer was then gently moved cephalad or caudad and angulated until desirable images were obtained. After it had been ensured that the imaging was on the axis, two-dimensional targeted M-mode tracings were recorded at a paper speed of 50 mm/sec. A 1.4-Fr micromanometer-tipped catheter (Millar Instruments, Houston, TX) was inserted into the right carotid artery and then advanced into the LV to measure LV pressures.

2.6. Tissue preparation and histopathology

After the mice were sacrificed, the heart was excised and dissected into the right ventricle and LV including septum. From the LV tissues, 5-μm sections were cut and stained with Masson's trichrome. The myocyte cross-sectional area and collagen volume fraction were determined as described (Sobirin et al., 2012; Homma et al., 2013; Furihata et al., 2016).

2.7. Myocardial MMP Activity

MMP-2 and -9 activities was determined in LV tissue using gelatin zymography kit (Primary Cell Co. Ltd., Sapporo, Japan) as we described (Sobirin et al., 2012). The were digitized, and the size-fractionated bands, which indicated proteolytic levels, were measured by the integrated optical density in a rectangular region of interest.

2.8. Quantitative reverse transcriptase-polymerase chain reaction

Gene expression levels were quantified by real-time reverse transcription PCR as described (Sobirin et al., 2012; Homma et al., 2013). Total RNA was extracted from LV with the use of QuickGene-810 (FujiFilm, Tokyo) according to the manufacturer's instructions. cDNA was synthesized with a high-capacity cDNA reverse transcription kit (Applied Biosystems, Foster City, CA). A TAqMan quantitative PCR was performed with the 7300 real-time PCR system (Applied Biosystems) to amplify samples for TNF-α, interferon (IFN)-γ, IL-4, IL-10, IL-6, C-C motif chemokine ligand 5 (CCL5), and CCL2 cDNA. These transcripts were normalized to GAPDH. The primers were purchased from Applied Biosystems.

2.9. Immunoblotting analysis of ERK1/2, JNK, MAPK, STAT3, and Human Antigen R

Cell lysis and immunoblotting were performed as described (Sobirin et al., 2012; Homma et al., 2013; Furihata et al., 2016). Equal amounts of protein extracted from LV tissue were separated by sodium dodecyl sulfate-polyacrylamide gel electrophoresis (SDS-PAGE), transferred to nitrocellulose membranes, and blotted with rabbit polyclonal antibodies against phospho-extracellular signal-regulated kinase (p-ERK1/2), phospho-c-Jun N-terminal kinase (p-JNK), phospho-p38 mitogen-activated protein kinase (p-MAPK), phospho-signal transducer and activator of transcription 3 (p-STAT3), and human antigen R (HuR; Millipore, Billerica, MA). Specific bands were labeled with enhanced chemiluminescence and visualized by exposure of the membranes to films. After exposure, the nitrocellulose membranes were blot-stripped using the Re-Blot Plus Western Blot Recycling Kit (Millipore) and re-blotted with rabbit polyclonal antibodies against ERK1/2, JNK, p38 MAPK, STAT3, and rabbit monoclonal antibodies against GAPDH. All antibodies except HuR were purchased from Cell Signaling Technology (Tokyo).

2.10. Immunohistochemistry of inflammatory cells

LV sections were immunostained with antibody against CD3 (Dako, Tokyo), MAC3 (BD Bioscience Pharmingen), and myeloperoxidase (MPO) (Dako), followed by counter-staining with Mayer's hematoxylin (Sobirin et al., 2012; Homma et al., 2013).

2.11. Statistical analysis

The data were expressed as the mean (SD). A survival analysis was performed by the Kaplan-Meier method, and between-group differences in survival were tested by the log-rank test. The normality of the data was examined using Shapiro-Wilk test. A between-group comparison of means was performed by two-way analysis of variance (ANOVA), followed by Tukey's test. Because some data were not normally distributed, their comparisons were tested with the Kruskal-Wallis test, followed by Dunn's comparisons. P-values <0.05 were considered significant.

3. RESULTS

3.1. iNKT cells

The flow cytometric analysis revealed that a small amount of iNKT cells were present in the LVs from WT+Sham mice. As expected, iNKT cells were not detected in LVs from the KO mice. The proportion of cardiac iNKT cells was increased in the WT+TAC group compared to the WT+Sham group (**Figure 1**).

3.2. Survival

No death was observed in the WT+Sham or KO+Sham mice. One WT+TAC mouse and one KO+TAC mouse died for unknown reasons, and five KO+TAC mice died of suspected HF during the 2 weeks after the TAC procedure. The survival rate up to 2 weeks was thus significantly lower in the KO+TAC mice compared to the WT+TAC mice (62.5% vs. 90.9%; $p<0.05$).

3.3. Echocardiography, hemodynamics, and organ weights

The echocardiographic parameters did not differ between the WT+Sham and KO+Sham mice. The LV wall thickness and LV mass/body weight were significantly increased without changes in LV diameters or fractional shortening in the WT+TAC mice at 2 weeks after the TAC **(Figure 2)**. The LV diameters were significantly greater and the LV fractional shortening was significantly lower in the KO+TAC mice compared to the WT+TAC mice. The LV wall thickness was comparable between the WT+TAC and KO+TAC groups. However, the LV mass/body weight was significantly increased in the KO+TAC mice compared to the WT+TAC mice.

The hemodynamics data and body and organ weights data are summarized in **Table 1**. The heart rate and aortic blood pressure were comparable among the four groups of mice. The LV systolic pressure was markedly elevated by the TAC procedure and significantly lower in the KO+TAC mice compared to the WT+TAC mice. Therefore, the pressure gradient over the TAC was not large in the KO+TAC group compared to the WT+TAC groups at 2 weeks after the TAC surgery. The LV end-diastolic pressure was significantly increased in the WT+TAC mice compared to the WT+Sham mice and tended to be exaggerated in the KO+TAC mice.

The LV +dP/dt and −dP/dt values also tended to be decreased in the KO+TAC group compared to the WT+TAC group, but the difference did not reach statistical significance. There was no significant difference in body weight among the four groups. In agreement with the echocardiographic LV mass/body weight, the heart weight/body weights and the LV weight/body weights were increased in the WT+TAC group compared to the WT+Sham group, and further increased in the KO+TAC group. Moreover, in accordance with the LV end-diastolic pressure, the lung weight/body weight (which is indicative of pulmonary congestion) tended to be increased in the WT+TAC mice and significantly increased in the KO+TAC mice.

3.4. Histopathology

The Masson's trichrome staining showed that the myocyte cross-sectional area and the collagen volume fraction were increased in the WT+TAC mice compared to the WT+Sham mice, and that these changes were significantly exacerbated in the KO+TAC mice (**Figure 3A–C**).

3.5. Myocardial MMP Activity

Representative gelatin zymography of the LV tissue from 4 groups was shown in **Figure 3D**. MMP-2 activity was increased in WT+TAC compared to WT+Sham mice, and this change was significantly increased in KO+TAC (**Figure 3E**). MMP-9 activity was not detected in 4 groups of mice.

3.6. Mitogen-activated protein kinases signal

Representative immunoblotting and summary data are shown in **Figure 4**. The ratio of p-ERK1/2 to total ERK1/2 (p-ERK/ERK) tended to be increased in the WT+TAC group compared to the WT+Sham group. It was significantly increased in the KO+Sham and KO+TAC groups, and the extent of the increase was greater in the KO+TAC group than in the KO+Sham group. The ratio of p-JNK and p-p38 MAPK to either total did not differ among the four groups of mice.

3.7. Cytokine gene expressions and cytokine signals

The IL-10 and TNF-α gene expression levels were significantly increased in the WT+TAC mice compared to the WT+Sham mice, and significantly reduced in the KO+TAC mice (**Figure 5A, B**). IL-6 was increased in the WT+TAC and KO+TAC groups, but did not differ significantly among the groups (**Figure 5C**). IFN-γ tended to be increased in the WT+TAC mice, and it was diminished in the KO mice (**Figure 5D**). IL-4 was not detected in any group.

The ratio of p-STAT3 to total STAT3 (p-STAT3/STAT3) was significantly increased in the TAC mice and was comparable between the WT+TAC and KO+TAC mice (**Figure 6**). The ratio of HuR/GAPDH was not significantly different among the four groups (**Figure 6**).

3.8. Immunohistochemistry staining of inflammatory cells and chemokines gene expression

The immunohistochemical stainings for MAC3 and CD3 were barely detectable in the LV tissue from both the WT+Sham and KO+Sham mice. In contrast, they were clearly increased in the WT+TAC and KO+TAC mice (**Figure 7A–D**). However, there was no significant difference in the infiltration of these cells between the WT+TAC and KO+TAC groups at 2 weeks after TAC. MPO-positive cells were not detected in the LV tissue from all groups of mice. CCL5 was increased in the WT+TAC and KO+TAC group but did not differ significantly among the groups (**Figure 8A**). CCL2 tended to be increased in the WT+TAC mice and was diminished in the KO mice (**Figure 8B**).

4. DISCUSSION

The most important finding of this study was that the disruption of iNKT cells exacerbated LV remodeling and hastened the transition to HF after the TAC procedure. iNKT cells generally account for a very small proportion of MNCs and have an abundant capacity to produce a mixture of T_H1 and T_H2 cytokines and a vast array of chemokines. Although there are only a few iNKT cells in the heart and the infiltration of iNKT cells in cardiac hypertrophy increases only slightly, the iNKT cells provide the basis for the transition from an immunologically chaotic condition to the ordered condition and orchestrate tissue inflammation. As a result, the infiltration and activation of iNKT cells may compensate for the development of HF.

The echocardiographic data showed that at 2 weeks after surgery, our TAC model exhibited compensated LV hypertrophy with preserved systolic LV function and without HF in wild-type mice. In KO mice, the TAC surgery clearly induced decompensated LV

hypertrophy with depressed systolic LV function and overt HF. We could not measure the pressure gradient over the aortic constriction immediately after the TAC surgery in the mice, but it was lower in the KO+TAC mice than in the WT+TAC mice at 2 weeks after the This suggests that in the KO+TAC mice, the low pressure gradient is due to the low LV function. In our preliminary experiment using other sets of WT+TAC and KO+TAC mice, there was no significant difference in the pressure gradient between the two groups immediately after the TAC operation. Therefore, the difference in cardiac phenotype between the WT+TAC and KO+TAC mice could not be explained by the difference in the pressure gradient.

We detected a small amount of iNKT cells in LV tissues using the same methods we reported, and our present findings confirm our previous results (Sobirin et al., 2012; Homma et al., 2013). Here, in a preliminary experiment conducted to validate the detection of iNKT cells by the flow cytometry analysis, we evaluated spleen MNCs. iNKT cells were clearly detected in the spleens from WT mice but not KO mice. Generally, the proportion of iNKT cells to MNCs is approx. 10%–20% in mouse liver, 1.5% in mouse spleen, 0.5% in mouse thymus, and 0.01%–0.5% in human peripheral blood (Lee et al., 2002a,b; Watarai et al., 2008). It is thus not surprising that a very small proportion of iNKT cells among MNCs was detected in the mouse hearts. The important point is that the iNKT cells are increased by approx. threefold in WT+TAC mice. The significance of this increase was revealed using KO mice in the present study.

The protective role of iNKT cells has been shown to include major two mechanisms: a shift from T_H1 toward a T_H2 pattern, and the induction of the immunosuppressive cytokine IL-10 in T_H1-like autoimmune diseases (Croxford et al., 2006). Our present findings also showed that IL-10 was increased in the LV from WT+TAC mice and decreased in the LV KO+TAC mice in association with the changes in iNKT cells. IL-10 can inhibit the of proinflammatory cytokines by macrophages and T_H1 cells and directly promote the death inflammatory cells (Forster et al., 1989; Fiorentino et al., 1991a, b). Beyond its suppressive effects on inflammatory gene synthesis, IL-10 could also regulate the extracellular matrix and angiogenesis (Lacraz et al., 1995; Silvestre et al., 2000; Apte et al., 2006; Dace et al., 2008). Krishnamurthy et al. showed that IL-10 suppressed inflammation and attenuated LV

remodeling after MI in mice by inhibiting fibrosis via the suppression of HuR and the activation of STAT3 (Krishnamurthy et al., 2009). However, we did not observe any significant differences in STAT3 activation or HuR expression between the WT+TAC and KO+TAC mice.

The present study also showed that TNF-α was increased in LV from WT+TAC mice and decreased in LV from KO+TAC mice. TNF-α is a proinflammatory cytokine that is considered to be cardiotoxic and induce LV dysfunction (Kubota et al., 1997; Sun et al., 2007). However, TNF-α also has protective effects during the maladaptive transition to HF (Hirota et al., 1999; Higuchi et al., 2004). Indeed, the treatment of patients with HF with either soluble TNF receptor (the RENEWAL study) or an anti-TNF antibody (the ATTACH trial) did not show clinical benefits (Chung et al., 2003; Mann et al., 2004). A decrease in the ratio of IL-10 to TNF-α was reported to correlate with depressed cardiac function (Kaur et al., 2006). These findings are consistent with our present observation that the ratio of mRNA expression of IL-10 to TNF-α was significantly less in the KO+TAC group compared to the WT+TAC group (0.54±0.14 vs. 1.47±0.23, $p<0.05$). These findings suggest that investigations of the underlying mechanisms of inflammation in the development of HF should focus on the modulation of the cytokine balance rather than on individual cytokines. Given that iNKT cells can function as a bridge between the innate and adaptive immune systems, they may act as an upstream regulator of the cytokine balance in the pressure-overloaded heart.

MMP-2 is ubiquitously distributed in cardiac myocytes and fibroblasts, and plays a crucial role in the development of cardiac remodeling in response to pressure overload (Cheung et al., 2000; Matsusaka et al., 2006). Our previous data showed that the selective disruption of the MMP-2 gene attenuated interstitial fibrosis in LV hypertrophy after TAC (Matsusaka et al., 2006). Therefore, it has been suggested that the activation of MMP-2 might play an important role in development of interstitial fibrosis in our model. However, the mechanisms responsible for the activation of MMP-2 by the deletion of iNKT cells remain to be determined.

The MAPKs signaling pathways consist of a sequence of successively functioning kinases that ultimately result in the dual phosphorylation and activation of p38, JNKs, and ERKs (Garrington & Johnson, 1999). Notably, the activation of the MEK1-ERK1/2 pathway

has been shown to induce cardiac hypertrophy, and the reduction of MEK-ERK1/2 activity inhibits interstitial fibrosis and cardiac dysfunction in vivo (Bueno et al., 2000; Thum et al., 2008). We demonstrated that the phosphorylation of ERKs was significantly increased in KO mice compared to WT mice, and it was markedly enhanced in KO+TAC mice. These data thus indicate that ERKs signaling might be one of the regulatory factors in the exacerbation of myocyte hypertrophy and interstitial fibrosis after TAC in KO mice. MAPKs are regulated by reversible phosphorylation, and this is due to phosphatase-mediated dephosphorylation by MAPK phosphatases (MKP) (Keyse, 2000). The overexpression of MKP-1 can inhibit cardiac hypertrophy via the dephosphorylation of ERK, and the downregulation of MKP-1 can lead to cardiac hypertrophy via the phosphorylation of ERK (Hayashi et al., 2004). Immunological factors have been noted to alter MKP-1 expression (Wancket et al., 2012). Pro-inflammatory cytokines negatively express MKP-1, and anti-inflammatory cytokines positively express MKP-1. Therefore, the enhanced phosphorylation of ERK in KO+TAC mice may be due to a down-regulation of MKP-1 by disordered immunological conditions.

There are several limitations to be acknowledged in the present study. First, we could not show the conclusive role of iNKT cells in the development of cardiac remodeling after TAC, even if we performed the experiments using iNKT cells KO mice. Most ideal method to clarify this issue is a rescue experiment using adoptive transfer of iNKT cells to KO mice. Unfortunately, we could not complete this experiment due to technical difficulties. Second, we could not show clear evidence about the role of other immune cells in the exacerbation of cardiac remodeling in iNKT KO mice. Weisheit et al reported that macrophages and neutrophils were increased in the heart at 3 to 6 days after TAC (Weisheit et al., 2014). At 21 days after TAC, these tended to be increased, but were not significantly different. In particular, accumulation of $Ly6C^{low}$ macrophages, tissue repairing macrophages, was dominant. Nevers et al reported that T cells were increased in the heart at 2 to 4 weeks, but not 48 hours after TAC (Nevers et al., 2015). They also showed that neutrophils and macrophages in the heart did not differ at 48 hours, 2 weeks, and 4 weeks after TAC. They clarified using T cell deficient mice that the infiltration of T cells in the heart played a crucial role in the development of cardiac remodeling after TAC. iNKT cell-derived cytokines can activate many immune cells including T cells, macrophages and neutrophils (Kronenberg et al., 2002). Therefore, the changes in cardiac phenotype we observed in iNKT cells KO mice

may be associated with the changes in macrophages and T cells at earlier time point than 2 weeks. Further investigations are required to elucidate the role of other immune cells. Finally, protein levels of several cytokines including TNF-α and IL-10 could not be detected in the heart by immunohistochemical staining and flow cytometry analysis like our previous study (Homma et al., 2013; Sobirin et al., 2012). This may be due to short half-life, and smaller amount of cytokines protein in the heart.

In summary, the results of the present study demonstrated, for the first time, that the disruption of iNKT cells exacerbated the development of cardiac remodeling and HF after transverse aortic constriction. This suggests that iNKT cells play a protective role against the HF that is due to pressure overload. Our findings provide new mechanistic insights and may provide a basis for a new therapeutic target for HF.

AUTHORS CONTRIBUTIONS

All experiments were conducted at the Department of Cardiovascular Medicine, Faculty of Medicine and Graduate School of Medicine, Hokkaido University. S.K. and H.T. conceived and designed the research. M.T., S.T., N.K., T.F., A.F., Y.O., and A.S. performed the experiments; M.T., S.T., and M.AS. analyzed the data; S.K., N.I., and K.I. interpreted the results of the experiments; M.T., S.K., and S.T. drafted the manuscript; N.K., T.F., M.AS., A.F., Y.O., N.I., K.I., and H.T. edited and revised the manuscript. All authors approved the final version of the manuscript and agree to be accountable for all aspects of the work in ensuring that questions related to the accuracy or integrity of any part of the work are appropriately investigated and resolved. All persons designated as authors quality for authorship, and all those who qualify for authorship are listed.

ACKNOWLEDGEMENTS

We thank Ms. Kaoruko Kawai for her technical assistance, and Drs. Masaru Taniguchi and Toshinori Nakayama for the professional advice.

GRANTS

This work was supported in part by grants from Japanese Grant-In-Aid for Scientific Research: JP26350879 (to S.K.), JP26750331 (S.T.), JP16K16607 (H.T.), JP17K15979 (T.F.), JP17K10137 (A.F.), and JP17H04758 (S.T.).

DISCLOSURES

No conflicts of interest, financial or otherwise, are declared by the authors.

REFERENCES

Apte, R.S., Richter, J., Herndon, J., & Ferguson, T.A. (2006). Macrophages inhibit neovascularization in a murine model of age-related macular degeneration. *PLOS Medine, 3,* e310.

Bueno, O.F., De Windt, L.J., Tymitz, K.M., Witt, S.A., Kimball, T.R., Klevitsky, R., … Molkentin, J.D. (2000). The MEK1-ERK1/2 signaling pathway promotes compensated cardiac hypertrophy in transgenic mice. *The EMBO Journal, 19,* 6341-6350.

Cheung, P.Y., Sawicki, G., Wozniak, M., Radomski, M.W., & Schulz, R. (2000). Matrix metalloproteinase-2 contributes to ischemia-reperfusion injury in the heart. *Circulation, 101,* 1833-1839.

Chung, E.S., Packer, M., Lo, K.H., Fasanmade, A.A., Willerson, J.T., & Anti-TNF Therapy Against Congestive Heart Failure Investigators. (2003). Randomized, double-blind, placebo-controlled, pilot trial of infliximab, a chimeric monoclonal antibody to tumor necrosis factor-alpha, in patients with moderate-to-severe heart failure: Results of the anti-TNF Therapy Against Congestive Heart Failure (ATTACH) trial. *Circulation, 107,* 3133-3140.

Croxford, J.L., Miyake, S., Huang, Y.Y., Shimamura, M., & Yamamura, T. (2006). Invariant V(alpha)19i T cells regulate autoimmune inflammation. *Nature Immunology, 7,* 987-994.

Cui, J., Shin, T., Kawano, T., Sato, H., Kondo, E., Toura, I., … Taniguchi, M. (1997). Requirement for Valpha14 NKT cells in IL-12-mediated rejection of tumors. *Science, 278,* 1623-1626.

Dace, D.S., Khan, A.A., Kelly, J., & Apte, R.S. (2008). Interleukin-10 promotes pathological angiogenesis by regulating macrophage response to hypoxia during development. *PLOS ONE, 3,* e3381.

Fiorentino, D.F., Zlotnik, A., Mosmann, T.R., Howard, M., & O'Garra, A. (1991a). IL-10 inhibits cytokine production by activated macrophages. *The Journal of Immunology, 147,* 3815-3822.

Fiorentino, D.F., Zlotnik, A., Vieira, P., Mosmann, T.R., Howard, M., Moore, K.W., & O'Garra, A. (1991b). IL-10 acts on the antigen-presenting cell to inhibit cytokine production by Th1 cells. *The Journal of Immunology, 146,* 3444-3451.

Fischer, P., & Hilfiker-Kleiner, D. (2007). Survival pathways in hypertrophy and heart failure: The gp130-STAT axis. *Basic Research in Cardiology, 102,* 393-411.

Forster, I., Vieira, P., & Rajewsky, K. (1989). Flow cytometric analysis of cell proliferation dynamics in the B cell compartment of the mouse. *International Immunology, 1,* 321-331.

Furihata, T., Kinugawa, S., Takada, S., Fukushima, A., Takahashi, M., Homma, T., … Tsutsui, H. (2016). The experimental model of transition from compensated cardiac hypertrophy to failure created by transverse aortic constriction in mice. *International Journal of Cardiology Heart & Vasculature, 11,* 24-28.

Garrington, T.P., & Johnson, G.L. (1999). Organization and regulation of mitogen-activated protein kinase signaling pathways. *Current Opinion in Cell Biology, 11,* 211-218.

Godfrey, D.I., MacDonald, H.R., Kronenberg, M., Smyth, M.J., & Van Kaer, L. (2004). NKT cells: What's in a name? *Nature Reviews Immunology, 4,* 231-237.

Hayashi, D., Kudoh, S., Shiojima, I., Zou, Y., Harada, K., Shimoyama, M., … Komuro, I. (2004). Atrial natriuretic peptide inhibits cardiomyocyte hypertrophy through mitogen-activated protein kinase phosphatase-1. *Biochemical and Biophysical Research Communications, 322,* 310-319.

Higuchi, Y., McTiernan, C.F., Frye, C.B., McGowan, B.S., Chan, T.O., & Feldman, A.M. (2004). Tumor necrosis factor receptors 1 and 2 differentially regulate survival, cardiac dysfunction, and remodeling in transgenic mice with tumor necrosis factor-alpha-induced cardiomyopathy. *Circulation, 109,* 1892-1897.

Hirota, H., Chen, J., Betz, U.A., Rajewsky, K., Gu, Y., Ross, J., … Chien, K.R. (1999). Loss of a gp130 cardiac muscle cell survival pathway is a critical event in the onset of heart failure during biomechanical stress. *Cell, 97,* 189-198.

Homma, T., Kinugawa, S., Takahashi, M., Sobirin, M.A., Saito, A., Fukushima, A., … Tsutsui, H. (2013). Activation of invariant natural killer T cell.s by alpha-galactosylceramide ameliorates myocardial ischemia/reperfusion injury in mice. *Journal of Molecular and Cellular Cardiology, 62,* 179-188.

Hong, S., Wilson, M.T., Serizawa, I., Wu, L., Singh, N., Naidenko, O.V., … Van Kaer, L. (2001). The natural killer T-cell ligand alpha-galactosylceramide prevents autoimmune diabetes in non-obese diabetic mice. *Nature Medicine, 7,* 1052-1056.

Kaur, K., Sharma, A.K., & Singal, P.K. (2006). Significance of changes in TNF-alpha and IL-10 levels in the progression of heart failure subsequent to myocardial infarction. *American Journal of Physiology Heart & Circulatory Physiology, 291,* H106-113.

Kawano, T., Cui, J., Koezuka, Y., Toura, I., Kaneko, Y., Motoki, K., … Taniguchi, M. (1997). CD1d-restricted and TCR-mediated activation of valpha14 NKT cells by glycosylceramides. *Science, 278,* 1626-1629.

Keyse, SM. (2000). Protein phosphatases and the regulation of mitogen-activated protein kinase signalling. *Current Opinion in Cell Biology, 12,* 186-192.

Krishnamurthy, P., Rajasingh, J., Lambers, E., Qin, G., Losordo, D.W., & Kishore, R. (2009). IL-10 inhibits inflammation and attenuates left ventricular remodeling after myocardial infarction via activation of STAT3 and suppression of HuR. *Circulation Ressearch, 104,* e9-18.

Kronenberg, M., & Gapin, L. (2002). The unconventional lifestyle of NKT cells. *Nature Reviews Immunology, 2,* 557-568.

Kubota, T., McTiernan, C.F., Frye, C.S., Slawson, S.E., Lemster, B.H., Koretsky, A.P., … Feldman, A.M. (1997). Dilated cardiomyopathy in transgenic mice with cardiac-specific overexpression of tumor necrosis factor-alpha. *Circulation Research, 81,* 627-635.

Lacraz, S., Nicod, L.P., Chicheportiche, R., Welgus, H.G., & Dayer, J.M. (1995). IL-10 inhibits metalloproteinase and stimulates TIMP-1 production in human mononuclear phagocytes. *The Journal of Clinical Investigation, 96,* 2304-2310.

Lee, P.T., Benlagha, K., Teyton, L., & Bendelac, A. (2002a). Distinct functional lineages of human V(alpha)24 natural killer T cells. *The Journal of Experimental Medicine, 195,* 637-641.

Lee, P.T., Putnam, A., Benlagha, K., Teyton, L., Gottlieb, P.A., & Bendelac, A. (2002b). Testing the NKT cell hypothesis of human IDDM pathogenesis. *The Journal of Clinical Investigation, 110,* 793-800.

Mann, D.L., McMurray, J.J., Packer, M., Swedberg, K., Borer, J.S., Colucci, W.S., … Fleming, T. (2004). Targeted anticytokine therapy in patients with chronic heart failure: Results of the Randomized Etanercept Worldwide Evaluation (RENEWAL). *Circulation, 109,* 1594-1602.

Matsuda, J.L., Mallevaey, T., Scott-Browne, J., & Gapin, L. (2008). CD1d-restricted iNKT cells, the 'Swiss-Army knife' of the immune system. *Current Opinion in Immunology, 20,* 358-368.

Matsusaka, H., Ide, T., Matsushima, S., Ikeuchi, M., Kubota, T., Sunagawa, K., … Tsutsui, H. (2006). Targeted deletion of matrix metalloproteinase 2 ameliorates myocardial remodeling in mice with chronic pressure overload. *Hypertension, 47,* 711-717.

Miellot, A., Zhu, R., Diem, S., Boissier, M.C., Herbelin, A., & Bessis, N. (2005). Activation of invariant NK T cells protects against experimental rheumatoid arthritis by an IL-10-dependent pathway. *European Journal of Immunology, 35,* 3704-3713.

Nevers, T., Salvador, A.M., Grodecki-Pena, A., Knapp, A., Velázquez, F., Aronovitz, M., … Alcaide, P, (2015). Left ventricular T-cell recruitment contributes to the pathogenesis of heart failure. *Circulation: Heart Failure, 8,* 776-787.

Nicoletti, A., & Michel, J.B. (1999). Cardiac fibrosis and inflammation: interaction with hemodynamic and hormonal factors. *Cardiovascular Research, 41,* 532-543.

Rogers, L., Burchat, S., Gage, J., Hasu, M., Thabet, M., Willcox, L., … Whitman, S.C. (2008). Deficiency of invariant V alpha 14 natural killer T cells decreases atherosclerosis in LDL receptor null mice. *Cardiovascular Research, 78,* 167-174.

Sharif, S., Arreaza, G.A., Zucker, P., Mi, Q.S., Sondhi, J., Naidenko, O.V., … Herbelin, A. (2001). Activation of natural killer T cells by alpha-galactosylceramide treatment prevents the onset and recurrence of autoimmune Type 1 diabetes. *Nature Medine, 7,* 1057-1062.

Silvestre, J.S., Mallat, Z., Duriez, M., Tamarat, R., Bureau, M.F., Scherman, D., … Levy, B.I. (2000). Antiangiogenic effect of interleukin-10 in ischemia-induced angiogenesis in mice hindlimb. *Circulation Research, 87,* 448-452.

Singh, A.K., Wilson, M.T., Hong, S., Olivares-Villagomez, D., Du, C., Stanic, A.K., … Van Kaer, L. (2001). Natural killer T cell activation protects mice against experimental autoimmune encephalomyelitis. *The Journal of Experimental Medicine, 194,* 1801-1811.

Sobirin, M.A., Kinugawa, S., Takahashi, M., Fukushima, A., Homma, T., Ono, T., … Tsutsui, H. (2012). Activation of natural killer T cells ameliorates postinfarct cardiac remodeling and failure in mice. *Circulation Research, 111,* 1037-1047.

Sun, M., Chen, M., Dawood, F., Zurawska, U., Li, J.Y., Parker, T., … Liu, P.P. (2007). Tumor necrosis factor-alpha mediates cardiac remodeling and ventricular dysfunction after pressure overload state. *Circulation, 115,* 1398-1407.

Takada, S., Masaki, Y., Kinugawa, S., Matsumoto, J., Furihata, T., Mizushima, W., … Tsutsui, H. (2016). Dipeptidyl peptidase-4 inhibitor improved exercise capacity and mitochondrial biogenesis in mice with heart failure via activation of glucagon-like peptide-1 receptor signalling. *Cardiovascular Research, 111,* 338-347.

Thum, T., Gross, C., Fiedler, J., Fischer, T., Kissler, S., Bussen, M., … Engelhardt, S. (2008). MicroRNA-21 contributes to myocardial disease by stimulating MAP kinase signalling in fibroblasts. *Nature, 456,* 980-984.

Wancket, L.M., Frazier, W.J., & Liu, Y. (2012). Mitogen-activated protein kinase phosphatase (MKP)-1 in immunology, physiology, and disease. *Life Sciences, 90,* 237-248.

Watarai, H., Nakagawa, R., Omori-Miyake, M., Dashtsoodol, N., & Taniguchi, M. (2008). Methods for detection, isolation and culture of mouse and human invariant NKT cells. *Nature Protocols, 3,* 70-78.

Weisheit, C., Zhang, Y., Faron, A., Köpke, O., Weisheit, G., Steinsträsser, A., … Baumgarten, G. (2014). Ly6C(low) and not Ly6C(high) macrophages accumulate first in the heart in a model of murine pressure-overload. *PLOS ONE, 9,* e112710.

Xia, Y., Lee, K., Li, N., Corbett, D., Mendoza, L., & Frangogiannis, N.G. (2009). Characterization of the inflammatory and fibrotic response in a mouse model of cardiac pressure overload. *Histochemistry and Cell Biology, 131,* 471-481.

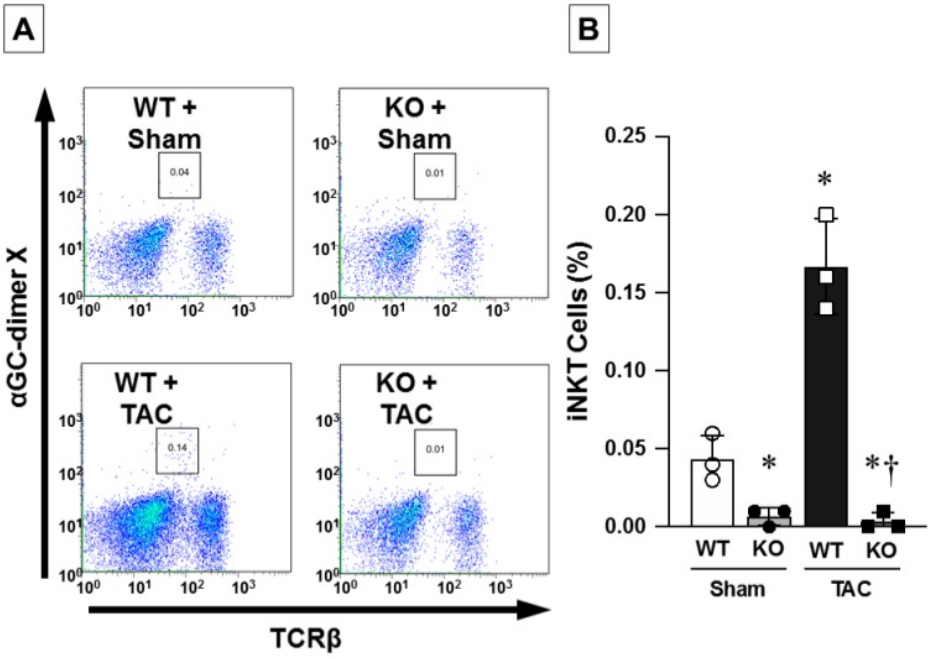

FIGURE 1 Cardiac iNKT cells were increased after TAC

A: Representative flow cytometric assessment of cardiac mononuclear cells obtained from WT+Sham, KO+Sham, WT+TAC, and KO+TAC mice. Cardiac mononuclear cells from five different mice from each group were pooled and analysed. Squares indicate the population of iNKT cells. **B**: The proportion of cardiac iNKT cells to mononuclear cells. n=3 for each group. Data are mean (SD). *p<0.05 vs. WT+Sham, †p<0.05 vs. WT+TAC.

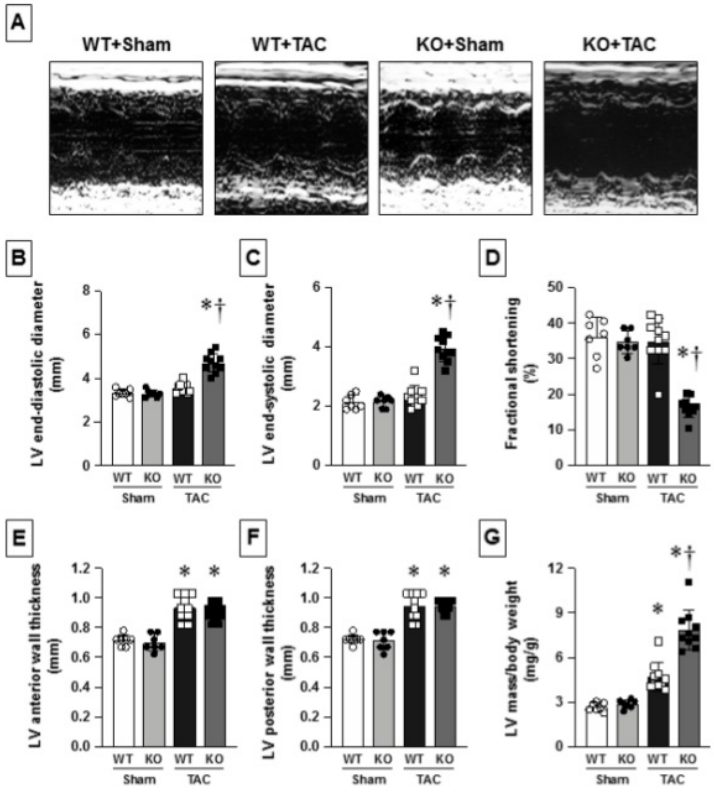

FIGURE 2 The disruption of iNKT cells exacerbated LV remodeling

A: Representative echocardiographic images in WT+Sham, KO+Sham, WT+TAC, and KO+TAC mice. **B-G:** Summary data for echocardiographic parameters in WT+Sham (n=7), KO+Sham (n=7), WT+TAC (n=10), and KO+TAC (n=10) mice at 2 weeks after TAC surgery. Data are mean (SD). *p<0.05 vs. WT+Sham, †p<0.05 vs. WT+TAC.

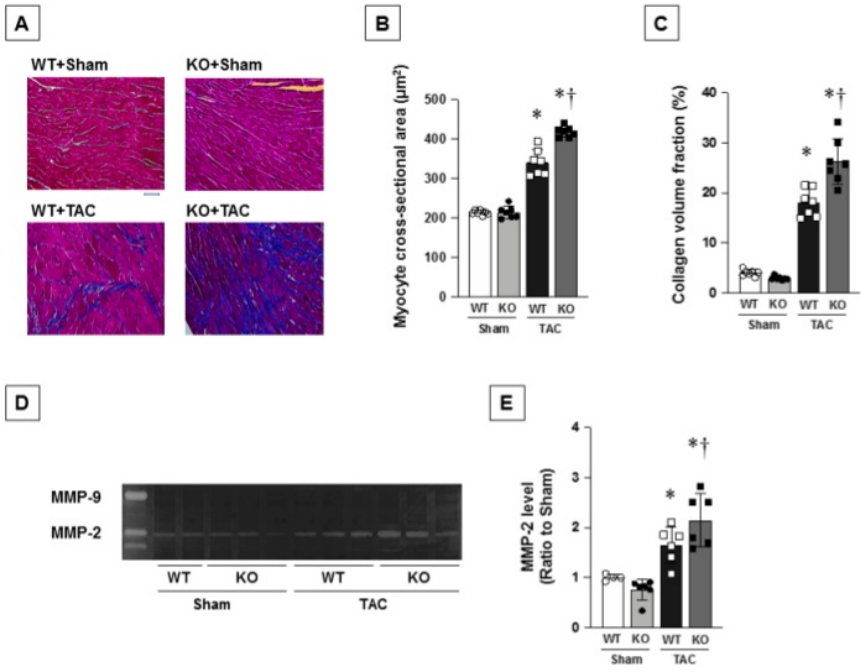

FIGURE 3 The disruption of iNKT cells exacerbated cardiac hypertrophy and interstitial fibrosis.

A: Representative high-power photomicrographs of LV cross-sections stained with Masson's trichrome from WT+Sham, KO+Sham, WT+TAC, and KO+TAC mice. Scale bar, 50 μm. **B, C:** Myocyte cross-sectional area and collagen volume fraction were analyzed in four groups of mice (n=7 each). **D, E**: Representative LV zymographic MMP-2 and MMP-9 activities in LV and densitometric analysis of MMP-2 (n= 4-6 for each). Data are mean (SD). *P<0.05 vs. WT+Sham, †P<0.05 vs WT+TAC.

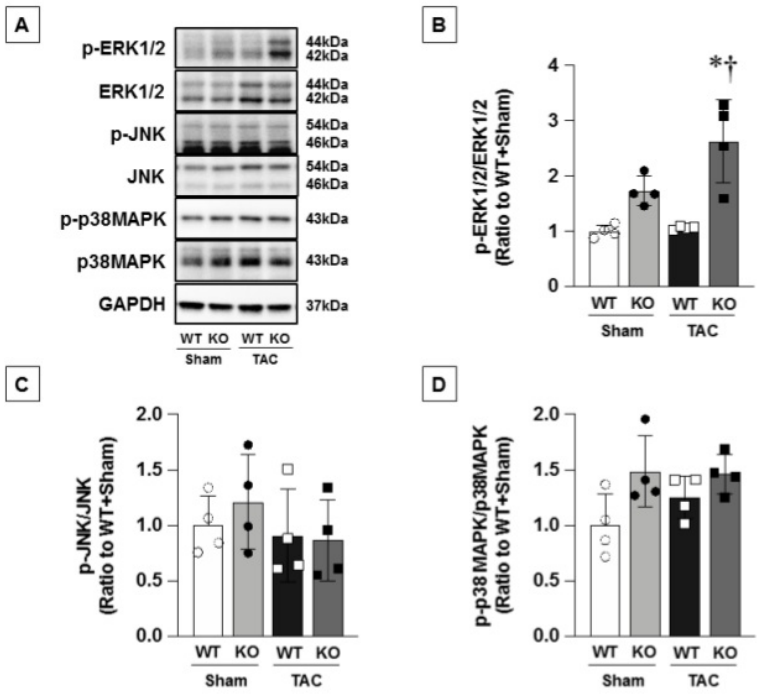

FIGURE 4 The disruption of iNKT cells increased phosphorylation of ERK1/2

A-D: Representative immunoblotting analysis and the summary data for p-ERK1/2/ERK1/2, p-JNK/JNK, and p-p38MAPK/p38MAPK in LV tissues from WT+Sham, KO+Sham, WT+TAC, and KO+TAC mice (n=4 each). Data are mean (SD). *p<0.05 vs. WT+Sham, †p<0.05 vs WT+TAC.

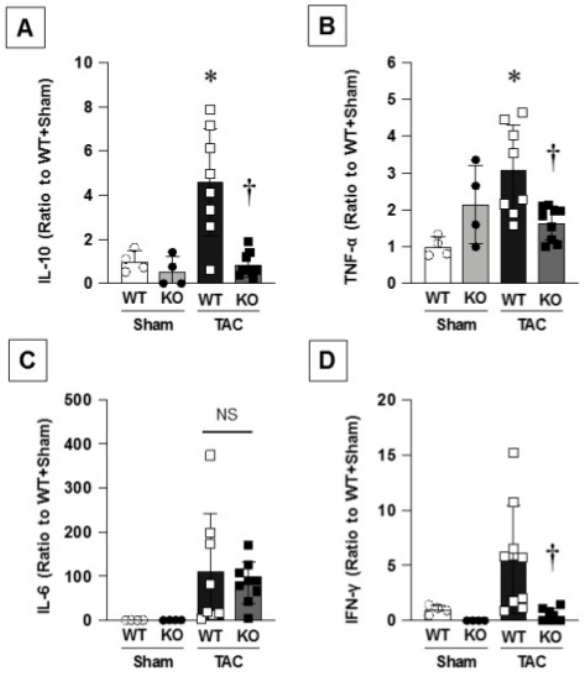

FIGURE 5 The disruption of iNKT cells altered mRNA expressions of cytokines

A-D: Quantitative analysis of the mRNA expressions of IL-10, TNF-α, IL-6, and IFN-γ in the LV from the four groups of mice (n=4–9 for each). The mRNA expressions were normalized to GAPDH expression and are depicted as the ratio to WT+Sham. Data are mean (SD). *p<0.05 vs. WT+Sham, †p<0.05 vs WT+TAC.

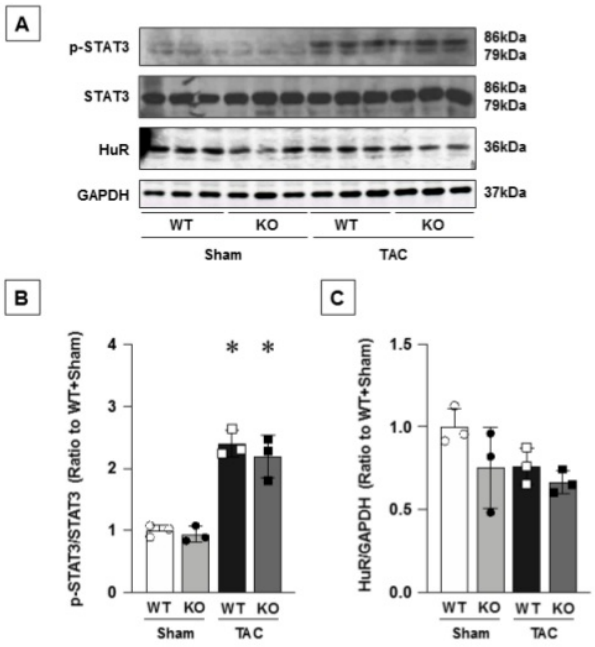

FIGURE 6 The disruption of iNKT cells did not affect cytokine signals

A-C: Representative immunoblotting analysis and the summary data for p-STAT3/STAT3 and HuR/GAPDH in LV tissues from the four groups of mice (n=3 each). Data are mean (SD). *p<0.05 vs. WT+Sham.

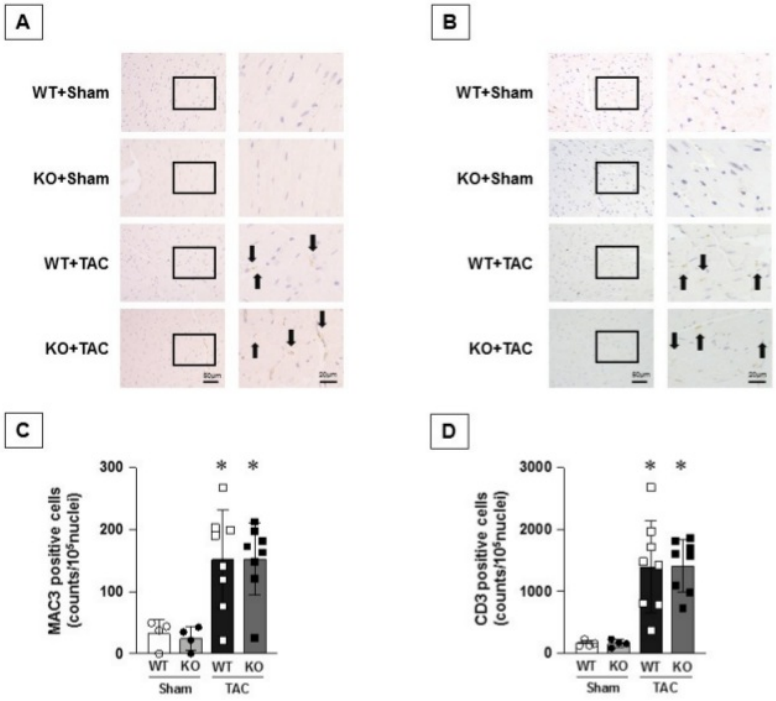

FIGURE 7 The disruption of iNKT cells did not affect the infiltration of MAC-3 positive and CD-3 positive cells at 2 weeks

A, B: Representative photomicrographs of LV cross-sections stained with anti MAC-3 and anti CD3 in WT+Sham, KO+Sham, WT+TAC, and KO+TAC mice. Each right panel shows a zoom image of square portion in each left panel. *Black arrows*: Positive-staining cells. **C, D:** Summary data of the numbers of MAC-3-positive and CD3-positive cells in the LV (n=4–8 for each). Data are mean (SD). *p<0.05 vs. WT+Sham.

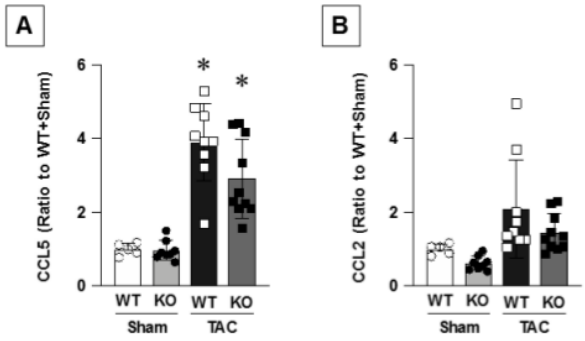

FIGURE 8 The disruption of iNTK cells did not affect the mRNA expressions of CCL5 and CCL2

A, B: Quantitative analysis of the mRNA expressions of CCL5 and CCL2 in the LV from the four groups of mice (n=5–10 each). The mRNA expressions were normalized to the GAPDH expression and are depicted as the ratio to WT+Sham. Data are mean (SD). *p<0.05 vs. WT+Sham.

Table 1. Hemodynamics, body weight, and organ weights at 2 weeks after TAC

	WT+Sham	KO+Sham	WT+TAC	KO+TAC
Hemodynamics:				
n	4	4	10	7
Heart rate, bpm	498 (20)	474 (31)	479 (38)	488 (61)
Aortic systolic BP, mmHg	95 (2)	99 (6)	96 (22)	93 (13)
Aortic diastolic BP, mmHg	63 (4)	71 (8)	73 (10)	68 (19)

LV systolic pressure, mmHg	99 (6)	101 (4)	198 (22)*	164 (24)*†
LV end-diastolic pressure, mmHg	1.4 (0.6)	1.8 (1.0)	5.4 (1.6)*	7.3 (2.4)*
LV +dP/dt, mmHg/sec	8752 (861)	9992(1530)	10695 (1695)	7526 (1244)
LV -dP/dt, mmHg/sec	7540 (1406)	6829 (1140)	8669 (1803)	6548 (1214)
Body and organ weights:				
n	7	7	10	10
Body weight, g	25.8 (1.7)	24.8 (2.6)	26.0 (2.1)	24.6 (1.3)
Heart weight/body weight, mg/g	4.8 (0.4)	5.1 (0.5)	7.2 (1.3)*	10.0 (0.7)*†
LV weight/body weight, mg/g	3.6 (0.3)	3.7 (0.4)	5.6 (1.0)*	7.6 (0.7)*†
Lung weight/body weight, mg/g	5.5 (0.3)	5.2 (0.4)	7.8 (4.5)	14.6 (4.4)*†

Data are mean (SD). *p<0.05 vs. WT+Sham, †p<0.05 vs WT+TAC. LV, left ventricle; BP, blood pressure.

The disruption of invariant natural killer T cells exacerbates cardiac hypertrophy and failure due to pressure overload in mice

ORIGINALITY REPORT

3%	3%	5%	%
SIMILARITY INDEX	INTERNET SOURCES	PUBLICATIONS	STUDENT PAPERS

PRIMARY SOURCES

1	Ian B. Stewart, Brittany Dias, David N. Borg, Aaron J. E. Bach, Beatrix Feigl, Joseph T. Costello. "Intraocular Pressure Is a Poor Predictor of Hydration Status following Intermittent Exercise in the Heat", Frontiers in Physiology, 2017 Publication	1%
2	Takahiro Inoue, Tomomi Ide, Mayumi Yamato, Masayoshi Yoshida et al. "Time-dependent changes of myocardial and systemic oxidative stress are dissociated after myocardial infarction", Free Radical Research, 2009 Publication	1%
3	Role of Proteases in Cellular Dysfunction, 2014. Publication	1%

Exclude quotes	On	Exclude matches	< 1%
Exclude bibliography	On		

The disruption of invariant natural killer T cells exacerbates cardiac hypertrophy and failure due to pressure overload in mice

GRADEMARK REPORT

FINAL GRADE

/0

GENERAL COMMENTS

Instructor

PAGE 1

PAGE 2

PAGE 3

PAGE 4

PAGE 5

PAGE 6

PAGE 7

PAGE 8

PAGE 9

PAGE 10

PAGE 11

PAGE 12

PAGE 13

PAGE 14

PAGE 15

PAGE 16

PAGE 17

PAGE 18

PAGE 19

PAGE 20

PAGE 21

PAGE 22

PAGE 23

PAGE 24

PAGE 25

PAGE 26

PAGE 27

PAGE 28

PAGE 29

PAGE 30

PAGE 31

PAGE 32